THE JOURNAL OF BIOLOGICAL CHEMISTRY VOL. 286, NO. 23, pp. 20688–20700, June 10, 2011
Printed in the U.S.A.

RNA Binding Targets Aminoacyl-tRNA Synthetases to Translating Ribosomes*[S]

Received for publication, December 5, 2010, and in revised form, April 1, 2011 Published, JBC Papers in Press, April 1, 2011, DOI 10.1074/jbc.M110.209452

Alexandre David[‡], Nir Netzer[‡], Michael Brad Strader[§], Suman R. Das[‡], Cai Yun Chen[§], James Gibbs[‡], Philippe Pierre[¶], Jack R. Bennink[‡], and Jonathan W. Yewdell[‡1]

From the [‡]Laboratory of Viral Diseases, NIAID and the [§]Laboratory of Neurotoxicology, NIMH, National Institutes of Health, Bethesda, Maryland 20892 and the [¶]Centre d'Immunologie de Marseille Luminy, Marseille, France

Here, we examine tRNA-aminoacyl synthetase (ARS) localization in protein synthesis. Proteomics reveals that ten of the twenty cytosolic ARSs associate with ribosomes in sucrose gradients: phenylalanyl-RS (FRS), and the 9 ARSs that form the multi-ARS complex (MSC). Using the ribopuromycylation method (RPM) for localizing intracellular translation, we show that FRS and the MSC, and to a lesser extent other ARSs, localize to translating ribosomes, most strikingly when translation is restricted to poxvirus or alphavirus factories in infected cells. Immunoproximity fluorescence indicates close proximity between MSC and the ribosome. Stress induced-translational shutdown recruits the MSC to stress-granules, a depot for mRNA and translation components. MSC binding to mRNA provides a facile explanation for its delivery to translating ribosomes and stress granules. These findings, along with the abundance of the MSC (9×10^6 copies per cell, roughly equimolar with ribosomes), is consistent with the idea that MSC specificity, recently reported to vary with cellular stress (Netzer, N., Goodenbour, J. M., David, A., Dittmar, K. A., Jones, R. B., Schneider, J. R., Boone, D., Eves, E. M., Rosner, M. R., Gibbs, J. S., Embry, A., Dolan, B., Das, S., Hickman, H. D., Berglund, P., Bennink, J. R., Yewdell, J. W., and Pan, T. (2009) *Nature* 462, 522–526) can be modulated at the level of individual mRNAs to modify decoding of specific gene products.

Protein translation is a highly choreographed process performed by a number of remarkable enzymes, including ribosomes and aminoacyl-tRNA synthetases (ARSs).[2] ARSs catalyze the attachment of amino acids to their cognate tRNAs by an amino-acyl bond (1). The eukaryotic cell cytosol has 20 ARSs, each highly specific for one of the 20 standard amino acids used in synthesis. Mitochondria use a largely non-overlapping set of nuclear gene encoded ARSs for their own unique translation machinery. Ten ARSs (designated by single letter amino acid) code as ARS: EPRS (ERS and PRS are present in a single protein), DRS, IRS, KRS, LRS, MRS, QRS, RRS) form a single complex (2, 3), associated with 3 accessory components (p18, p38, p43) to create the multi-aminoacyl-tRNA synthetase complex (MSC) (4).

MSC is likely present in all eukaryotic cells, but has not been found in bacterial or archaeal cells (5). The MSC may exist as a complex in part to control the non-canonical functions of its components, many of which are known to perform alternative duties ranging from suppressing translation to regulating apoptosis, inflammation or angiogenesis (6). More directly related to its primary function, the MSC may optimize translation by coordinating synthetase activities to facilitate channeling of tRNA to ribosomes, a concept championed by Deutscher and co-workers (7, 8). Consistent with this idea, the MSC is known to co-sediment with both free and membrane-bound ribosomes (9–11).

It has been known for decades that active ribosomes are either docked to the endoplasmic reticulum (ER) or free in the cytosol (mitochondria possess unique ribosomes translating 13 mitochondrial genes). It has generally been assumed that ER-bound ribosomes exclusively translate proteins that are exported into the ER via signal sequences that dock ribosomes to the ER (12). Nicchitta and co-workers (13–17) have provided compelling evidence that a large subset of ER-bound ribosomes translates proteins lacking signal sequences that are targeted to the cytosol or nucleus. ER bound *versus* cytosolic ribosomes can be physically separated based on the diffusion of cytosolic ribosomes from live cells treated with digitonin (Dig) (18).

Our interest in aminoacyl synthetase function was prompted by our recent discovery that the fidelity of Met attachment to tRNA is decreased up to 10-fold in cultured cells following their infection with a variety of viruses, activation of innate immune receptors, or exposure to chemical stress (19). To better understand this phenomenon, we have characterized the distribution and function of ARSs in unperturbed cells and cells subjected to infectious and chemical stress. Our findings have broad implications for the function of ARSs in translation and translational shut down in normal cells and cells experiencing infectious, chemical, or physical stress.

* This work was supported, in whole or in part, by the Division of Intramural Research, NIAID, National Institutes of Health.

[S] The on-line version of this article (available at http://www.jbc.org) contains supplemental Figs. S1–S4 and Tables S1 and S2.

[1] To whom correspondence should be addressed: NIAID, Building 33, 33 North Dr., National Institutes of Health, Bethesda, MD 20892. Tel.: 301-402-4602; Fax: 301-402-7362; Email: jyewdell@nih.gov.

[2] The abbreviations used are: ARS, aminoacyl-tRNA synthetase; MSC, aminoacyl-tRNA synthetase complex; As, arsenite; CHX, cycloheximide; DIG, digitonin; DRC, Dig-resistant compartment; DRS, arginyl-RS; ER, endoplasmic reticulum; FRAP, fluorescence recovery after photobleaching; FRS, phenylalanyl-RS; KRS, lysyl-RS; MRS, methionyl-RS; NP, nucleoprotein; NRS, asparaginyl-RS; Puro, puromycin; PLA, proximity ligation assay; RPM, ribopuromycylation method; SFV, Semliki Forest Virus; SRS, seryl-RS; YRS, tyrosyl-RS; VV, vaccinia virus; 1D LC MS/MS, reverse phase liquid chromatography tandem mass spectrometry.

EXPERIMENTAL PROCEDURES

Cells—HeLa and 293T cells were cultured in DMEM (Invitrogen, Carlsbad, CA) supplemented with 7.5% FBS (HyClone Laboratories, Logan, UT), at 37 °C, 9% COR2R. Cells were plated overnight in T75 or T165 flasks to yield ~80% confluence at the start of the experiment. We generated the stable KRS-myc expressing HeLa cell line by transfecting with a KRS-myc plasmid generously supplied by Dr Sunghoon Kim (Center for Medicinal Protein Network and Systems Biology, Seoul National University, Seoul).

Ribosome Purification—293T cells were pretreated 5 min with 100 μg/ml of CHX, before being collected, washed, and resuspended in ice cold homogenization buffer (50 mM Tris-HCl pH 7.5, 5 mM $MgCl_2$, 25 mM KCl, 0.2 M sucrose, 0.5% Nonidet P-40, 100 μg/ml CHX, EDTA-free protease inhibitors (Roche), 10 units/ml RNase Out (Invitrogen), DEPC water). We then stroked cells 10 times using a homogenizer on ice and the lysate was spun 20,000 × *g* for 10min at 4 °C. The cleared lysate was layered at a 1:1 ratio (v/v) over sucrose (50 mM Tris-HCl pH 7.5, 5 mM $MgCl_2$, 25 mM KCl, 2 M sucrose, 0.5% Nonidet P-40, 100 μg/ml CHX, EDTA-free protease inhibitors (Roche), 10 units/ml RNase Out (Invitrogen), DEPC water). After centrifugation at 100,000 × *g* for 24 h at 4 °C, pellets were resuspended in homogenization buffer and layered on 15–50% sucrose gradient in the same buffer without detergents. Following centrifugation at 35,000 rpm (Beckman, SW41.Ti) for 2.5 h at 4 °C, gradients were fractionated with absorbance measured continuously at 254 nm. Ribosomes fractions were pooled, and after pelleting at 100,000 × *g* for 5 h at 4 °C, were used for proteomic analysis.

Exposure of Cells to Virus and Stress—HeLa cells were infected with WR VV at a multiplicity of 1 or 10 pfu/cell in BSS/BSA medium, SFV at a multiplicity of 10 pfu/cell in BSS/BSA. After adsorption at 37 °C for 1h, infected monolayers were overlaid with DMEM containing 7.5% FBS and incubated for several more hours (depending on the experiment). To elicit oxidative stress, cells were treated with 500 μM sodium arsenite for 30 min to 1 h at 37 °C.

Cell Extraction—Extracts were prepared from HeLa cells by sequential detergent extraction based on a previous publication (Lerner and Nicchitta, 15). Briefly, cell monolayers were washed with PBS, and incubated for 5 min on ice with permeabilization buffer (50 mM Tris-HCl, pH 7.5, 5 mM $MgCl_2$, 25 mM KCl, 100 μg/ml CHX, EDTA-free protease inhibitors (Roche)), 10 units/ml RNase Out (Invitrogen)) containing 0.015% digitonin. The supernatant was recovered, and cells were rewashed once with permeabilization buffer. Permeabilized cell monolayers were then solubilized with an equal volume of permeabilization buffer containing 1% Nonidet P-40 for 5 min on ice. The supernatant (membrane-bound fraction) was recovered, and both DSC and DRC were loaded on SDS-PAGE gel.

Antibodies—Rabbit antibodies against KRS, MRS, EPRS, P18 were purchased from Abcam. Mouse anti-SRS antibodies were from Abnova. Mouse anti-puromycin mAb has been described (20). Goat anti-Hur was purchased from Santa Cruz Biotechnology. Human anti-ribosomal P antiserum was from Immunovision.

Immunofluorescence and Microscopy—Cells were cultured on glass coverslips. Puromycin pulses were performed by incubating cells with 50 μg/ml of puromycin for 5 min at 37 °C in the presence of 100 μg/ml of CHX. Cells were washed with cold PBS (supplemented with CHX) and extracted with digitonin supplemented permeabilization buffer as described in "cell extraction." Following a wash with cold permeabilization buffer, cells were fixed 15 min with 3% paraformaldehyde (PFA) at room temperature. To characterize the DRC, cells were extracted with digitonin as described for puromycin staining and then incubated for 15 min at room temperature with 3% PFA. PLA experiments were performed either alone or in combination with puromycin labeling according to the manufacturer's protocol (Olink). Immunofluorescence was performed using staining buffer (0.05% saponin, 10 mM glycine, 5% FBS, PBS) as previously described (21). Following immunostaining, cells were labeled with Hoechst 3358 (Molecular Probes). Coverslips were mounted onto glass slides with Fluoromount-G (SouthernBiotech). Images were acquired with a Leica TCS SP5 confocal microscope (LAS AF software) using the HCX PLAPO 63× objective (numerical aperture: 1.4). Images were processed with Adobe Photoshop using only level and contrast adjustments. Co-localization statistical analysis was performed uisng the ImageJ software JACoP plug-in. For deconvolution we used Huygens Essentials software (Version 3.6, Scientific Volume Imaging BV, Hilversum, The Netherlands). Imaris (Bitplane) was used for quantification and statistical analysis.

Measure of Translation Rate—HeLa cells were treated with either puromycin or a combination of puromycin and CHX with the same concentration used for immunofluorescence staining.

MSC Purification—HeLa cells expressing myc-KRS (and control HeLa cells) were fractionated as described in "ribosome purification." MSC-containing fractions were incubated overnight with anti-c-Myc agarose beads (Sigma). Beads were washed three times with sucrose-free homogenization buffer, and MSC was eluted using Tris-glycine buffer, pH 2.8.

MSC Quantification—The concentration of purified MSC was calculated using the DC Protein Assay (Bio-Rad). Known amounts of MSC were immunoblotted for KRS. ImageJ was used to quantitate each band, and the data were used to generate a standard curve using Prism software was used to draw a standard curve (supplemental Fig. 2*C*). In parallel, a known number of HeLa cells (17,600 cells/μl of lysis buffer) were lysed, diluted, immunoblotted, and the standard curve was used to quantitate the amount of MSC per cell. Only values within the initial part of the curve (in blue) were exploited for quantification. We used MSC MW, 1200 kDa to calculate the number of molecules per HeLa cell.

MSC-mRNA Binding Experiment—Four cDNAs were used for this experiment, two from cellular mRNA (ApoB, Rent-1), two from IAV mRNA (NA, PB1). Each served as a template for radiolabeled *in vitro* transcription using HiScribe T7 (New England Biolabs) and [^{32}P]UTP (Perkin Elmer). Samples were treated 15 min with TURBO DNase I (Ambion) at 37 °C and purified by phenol-chloroform extraction. In parallel, we purified MSC as described above, using 10^6 cells and 30 μl of anti-Myc beads per condition. Beads (control or MSC bound) and

each purified mRNA (~2 μg) were incubated for 40 min in at RT in RNA hybridization buffer (5 mM $MgCl_2$, 100 mM KCl, 1 mM DTT, 10 mM Tris-HCl pH7.4), washed three times with the same buffer and eluted by incubation with Laemmli sample buffer (Tris-HCl, 0.08 M, pH 6.8, glycerol 10%, SDS 2%, DTT 0.1 M) for 10 min at 95 °C. CPM of each sample (total mRNA labeling and elution) were measured using a Microbeta TriLux counter (Perkin Elmer). For competition experiments, we used different concentrations of yeast tRNA (Ambion) added to beads before addition of radiolabeled mRNA probe.

MSC Purification and Quantitative RT-PCR—We purified MSC as described in "MSC purification," except for the elution step. Raw RNA samples were extracted from beads briefly with Trizol (Invitrogen, Carlsbad, CA), followed by addition of 0.2× volume chloroform at 4 °C. An equal volume of 70% ethanol was added to the aqueous phase, followed by purification of RNA on RNeasy spin columns (Qiagen, Valencia, CA). RNA was quantitated with a nanodrop spectrophotometer (Thermo Scientific, Wilmington, DE). Equal amounts of RNA were reverse transcribed with Verso RT (Thermo Scientific, Surrey, UK). Primer sets consisted of VVTK forward (GGATCCATCATGAACGGCGGACATATTC) and VVTK reverse (ACGTTGAAATGTCCCATCGAG), resulting in a product of 354 nt. Human gene control primers were obtained from PrimerDesign Ltd, (Southampton, UK). RT-PCR was performed on an Eppendorf Mastercycler ep realplex (Eppendorf AG, Hamburg, DE) using Power SYBR Green Master Mix (Applied Biosystems, Carlsbad, CA).

Mass Spectrometry of Proteins—Gel lanes from either polyribosome samples or tRNA synthetase pull-downs were manually excised top to bottom into 20 ~2-mm bands. In-gel tryptic digestion and peptide extraction followed a modified version of a standard protocol recently described.(22) For 1D liquid chromatography tandem mass spectrometry (1D-LC-MS/MS) extracted peptides were resuspended in 5% acetonitrile and 0.1% formic acid. For the work in this report, three different Thermo mass spectrometers (Thermo Electron, San Jose, CA) coupled to the same type of precolumn and analytical column were used for data acquisition. Peptide samples from isolated polysomes were injected into either a Shimadzu LC-VP HPLC system (Shimadzu, Columbia, MD) coupled online to an ESI LCQ Classic quadrupole ion trap mass spectrometer or a Nano LC 1D Proteomics HPLC system (Eksigent, Dublin, CA) coupled online to a linear ion trap (LTQ)-Orbitrap mass spectrometer equipped with a Nanomate nanoelectrospray ionization source (Advion, Ithaca, NY). Samples from tRNA synthetase pull-downs were injected into the same type of Eksigent HPLC system coupled online to a separate LTQ mass spectrometer. After injection, all peptide samples were desalted and preconcentrated online with a nano-C18 precolumn (300 μM × 5 mm) and then separated using a 75 μm x 10 cm BetaBasic-18 PicoFrit analytical column (New Objective, Woburn, MA) connected to the nanospray source. A linear gradient was developed using a 400 nl/min flow rate. LC mobile phases were A: 95% water/5% acetonirile/0.1% formic acid, B: 20% water/80% acetonitrile/0.1% formic acid. Retained analyte were eluted by increasing the acetonitrile concentration to 60% (1.5% per min (LCQ) or 1.25% per min (LTQ)). All 1D LC/MS/MS experiments were operated such that spectra were acquired for 60 min in the data-dependent mode with dynamic exclusion enabled. The top 3 peaks (LCQ) and top 5 peaks (LTQ) in the 400–2000 m/z range of every MS survey scan were fragmented. Specifically for the LTQ-Orbitrap, survey spectra were acquired with 60000 resolution in the Orbi-mass analyzer and fragmented in the LTQ ion trap.

Informatics—Fragmentation spectra were searched using the Mascot search engine (Matrix Sciences, London, UK) against the Human data base (created from the Uniprot Knowledgebase release 14.8) containing the porcine trypsin sequence and the reverse decoy of all translated sequences concatenated. All used in this work are in the process of being submitted to the NCBI peptide data resource and an accession number will be provided shortly. Search parameters were as follows: trypsin specificity, 3 missed cleavages, carbamidomethylation static modification, methionine oxidation variable modification, and +1, +2, and +3 charge states. The LCQ and LTQ precursor ion mass tolerance was ± 2.0 Da and the fragment ion mass tolerance was ± 0.8 Da. For the LTQ-Orbitrap the precursor ion mass tolerance was ± 0.5 Da and the fragment ion mass tolerance was ± 0.8 Da. For the polyribosome data, a total of 6 separate purifications (6 gel lanes) were performed where 4 LCQ and 2 LTQ-Orbitrap datasets were acquired. In both cases these data gave similar protein identification results: although the number of spectra and peptides identified are higher for the LTQ-Orbitrap. For the tRNA synthetase pull-down data a total of 4 separate pull-downs and 2 negative controls were performed (6 gel lanes) where 6 LTQ datasets were acquired. All 6 polysome datasets were concatenated and the resulting peptide identifications were assembled into protein identifications using the in-house software MassSieve (23). MassSieve was also used to compare the four concatenated tRNA synthetase pull-down data with negative control data. MassSieve filters were adjusted to include only peptide identifications with Mascot Ion Scores equal to or exceeding their identity scores. This resulted in a calculated false positive discovery (FDR) rate of 1.0% for the polyribosome data and 2.6% for the tRNA synthetase pull-down data (FDR = $2\ N_d/(N_d + N_t)$; where N_d and N_t are the number of matched decoy and target peptides passing the above cutoff, respectively). In both experimental data sets, MassSieve was used for peptide and protein level parsimony comparisons. A minimum of 2 peptides was required for a protein to be considered sufficiently identified.

RESULTS

Quantitating ARS-ribosome Association in Sucrose Gradients—Various ARSs have been reported to be associated with ribosomes based on tRNA charging activity with different amino acids (10). We extended this observation is by performing 1D reverse phase liquid chromatography tandem (LC) mass spectrometry (MS/MS) to analyze proteins co-sedimenting with HeLa cell polysomes in sucrose gradients (Table 1 and supplemental Fig. S1). Using the algorithm Mascot to search MS/MS spectra against the human data base, we identified 10 out of the 20 tRNA synthetases. The nine defined synthetases of the MSC, and as anticipated from prior studies (24), FRS (the lone free ARS to form multimers, comprised of $\alpha_2\beta_2$ subunits) (25). We

TABLE 1

tRNA synthetases identified by 1D LC MS/MS analysis of polysome fractions

The 2nd column refers to the number of peptide identifications for each protein listed in column 1. Column 3 refers to the number of MS/MS spectra matched by Mascot to peptides in column 2, and the final column refers to the overall primary sequence represented by those peptide identifications. For example, 257 spectra were matched to 42 peptides representing 62% of the bifunctional aminoacyl-tRNA synthetase primary sequence. It should be noted that while a minimum of 2 peptides were generally required to positively identify a given protein, multiple spectra were matched to the single peptide identifications representing p43 and p18.

Protein name	Accession number	Peptide IDs	Matched spectra	% Sequence coverage
Bifunctional aminoacyl-tRNA synthetase	P07814	42	257	62
Isoleucyl-tRNA synthetase	P41252	22	118	24
Arginyl-tRNA synthetase	P54136	17	56	40
Aspartyl-tRNA synthetase	P14868	16	59	43
Glutaminyl-tRNA synthetase	P47897	7	19	11
Leucyl-tRNA synthetase	P41252	11	35	15
Lysyl-tRNA synthetase	Q15046	4	15	11
Methionyl-tRNA synthetase	P56192	10	48	19
Phenylalanyl-tRNA synthetase alpha chain	Q9Y285	8	79	25
Phenylalanyl-tRNA synthetase beta chain	Q9NSD9	15	65	35
Multisynthetase complex auxiliary component p38	Q13155	2	3	13
Multisynthetase complex auxiliary component p43[a]	Q12904	1	6	4
Multisynthetase complex auxiliary component p18[a]	043324	1	2	14

[a] A single peptide was matched by multiple spectra to these proteins.

additionally identified 80% of the ribosomal proteins for large and small subunits, qualitatively validating the ribosomal composition of our samples (see supplemental Table S1, *A* and *B*). All 10 synthetase components were identified by a similar array of ARS peptides in samples from cells infected with influenza A virus (IAV) (~75% of those identified in uninfected cells, supplemental Table S1*C*), demonstrating that IAV infection does not grossly interfere with the association between ribosomes and ARSs.

We next examined the co-sedimentation of ARSs with ribosomes by immunoblotting sucrose gradient fractions prepared from Nonidet P-40 extracts (Fig. 1*A*). SRS, as expected from previous studies (26), was present at the top of the gradient, consistent with its sedimentation free of binding partners. More than 90% of FRS co-sedimented with monosome and polysome fractions. We monitored MSC behavior using antibodies specific for KRS and MRS. Nearly 80% of the MSC sedimented independently of ribosomes as free complexes (fractions 3–5). Surprisingly, the bulk of ribosome associated MSCs were present in crescendo in the densest fractions (inversely proportional to S3 and ribosomal phosphoprotein (P) expression), therefore presenting an expression profile distinct from FRS and the overall polysome profile.

We more accurately quantitated MSC behavior by immunoblotting three pooled gradient fractions corresponding to soluble, MSC, and polysome fractions (Fig. 1*B*). This clearly showed that only a small fraction of the MSC (as identified by anti-KRS, -MRS, or -DRS antibodies) stably co-sediment with polysomes under these conditions. By contrast, FRS predominantly sediments with polysomes, while SRS and YRS do not detectably co-sediment with polysomes.

Based on their behavior in sucrose gradient fractionation, we conclude that the various ARSs can be divided into three categories. FRS, which predominantly associates stably with polysomes, the MSC, which tenuously associates with polysomes, and SRS, YRS, and likely (based on their absence in mass spectrometry analysis) the 8 other synthetases, which do not stably associate with ribosomes under these conditions.

MSC Is Concentrated in Cellular Translation Sites—The ARS-ribosome interaction in sucrose may not accurately reflect the situation in cells, particularly if the interaction is weak, transient, or dependent on active metabolic processes. To better gauge the interaction of ribosomes with ARSs, we examined their intracellular distribution by immunofluorescence. We used antibodies specific for MRS or KRS to characterize MSC, because these synthetases are nearly exclusively present in the MSC and not as individual ARSs (Fig. 1*B*).

MRS and KRS demonstrate a nearly identical intracellular distribution; each extensively co-localizing with ribosomes stained with human anti-ribosomal P antibody (Fig. 1*C*). The pattern of staining was typical of the ER. Treating cells with digitonin prior to fixation to remove cytosolic ribosomes, as described by Nicchitta and co-workers (13), resulted in almost perfect co-localization of KRS and MRS with ribosomes (Fig. 1*C*). Importantly, Dig extraction had little effect on the intensity of KRS and MRS staining, indicating that most MSC detected by immunofluorescence associates with the ER compartment. Immunoblotting confirmed that nearly all of the MSC resists Dig extraction (Fig. 2*E*). Interestingly, while SRS co-localizes extensively with KRS, it is largely extracted by Dig, both by immunofluorescence (Fig. 1*D*) and immunoblotting analysis (Fig. 2*D*). Proteasomes are also nearly completely Dig-extractable, demonstrating that not all large protein assemblies are Dig resistant (supplemental Fig. S1*B*).

We next correlated the distribution of ARSs with translating ribosomes using the ribopuromycylation method (RPM). RPM is based on incorporation of puromycin (Puro) into nascent chains, whose association with ribosomes is maintained by the presence of chain elongation inhibitors such as cycloheximide (CHX). We then visualize puromycylated ribosome associated-nascent chains via immunofluorescence with a Puro specific mAb after Dig treatment of live cells, which eliminates free Puro staining (Fig. 2*A*).

Puro extensively colocalizes with ER-associated ribosomes and KRS (Fig. 2*A*). Blocking translation by treating cells with the translation initiation inhibitor pactamycin (27), or the oxidizing agent arsenite (As) (28), completely inhibits Puro staining, demonstrating that it is a *bona fide* measure of active protein synthesis (Fig. 2, *B* and *C*). Importantly, translation inhibition induced by either treatment clearly reduces KRS staining of cytosol-depleted cells by releasing it into the cytosol, while modestly reducing ribosomal staining.

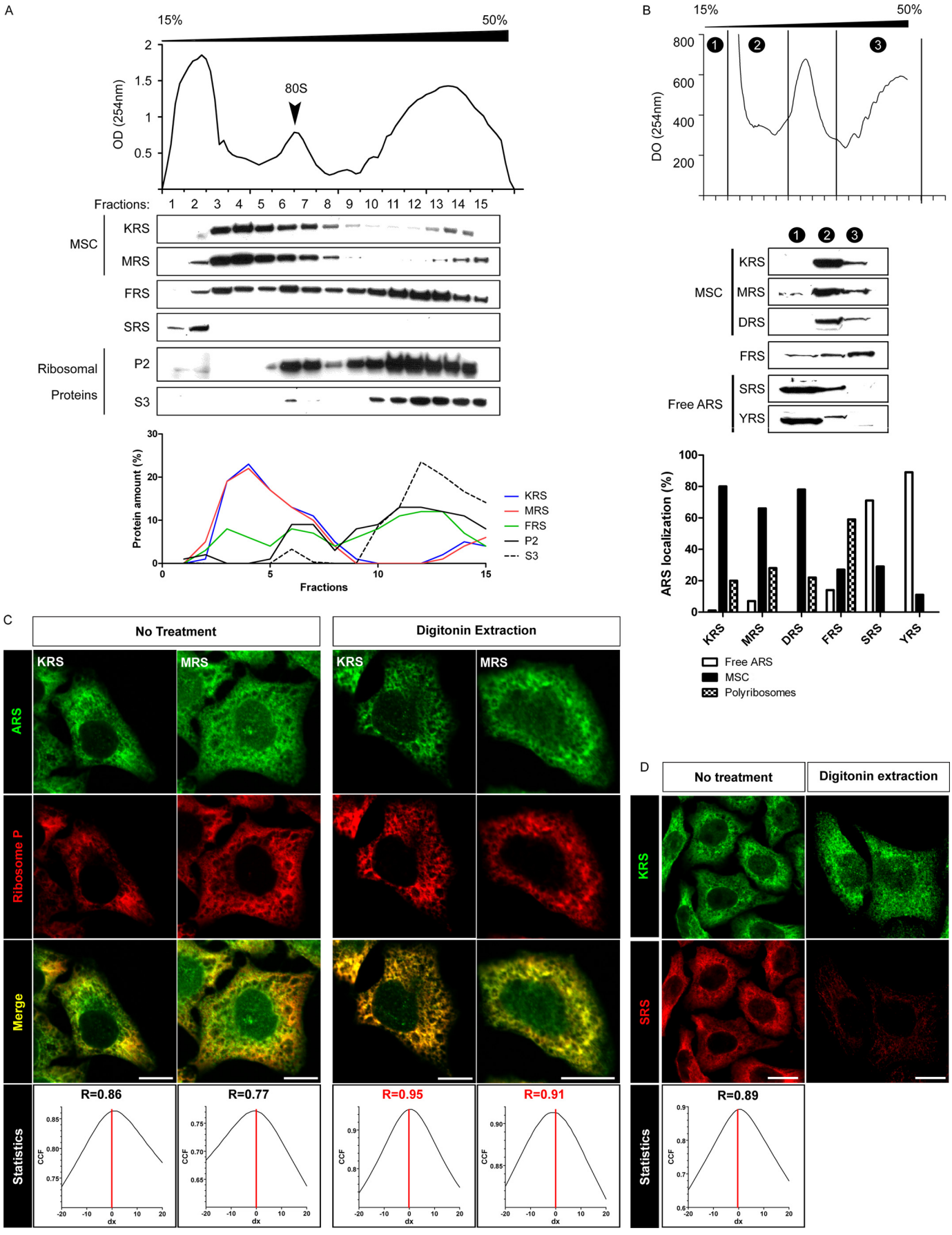
A
15%
50%
OD (254nm)
80S
Fractions: 1 2 3 4 5 6 7 8 9 10 11 12 13 14 15
MSC
KRS
MRS
FRS
SRS
Ribosomal Proteins
P2
S3
Protein amount (%)
Fractions
KRS
MRS
FRS
P2
S3
B
15%
50%
DO (254nm)
MSC
KRS
MRS
DRS
FRS
Free ARS
SRS
YRS
ARS localization (%)
Free ARS
MSC
Polyribosomes
C
No Treatment
Digitonin Extraction
ARS
Ribosome P
Merge
Statistics
R=0.86
R=0.77
R=0.95
R=0.91
D
No treatment
Digitonin extraction
KRS
SRS
Statistics
R=0.89

Using immunoblotting, we extended these findings to show that translational arrest has minor effects on the total amounts of KRS, MRS, FRS, SRS, ribosomes, or proteasomes recovered from cells (Fig. 2*D*). Importantly, both arsenite and pactamycin release KRS, MRS, FRS and ribosomes from the Dig resistant compartment (DRC) without increasing SRS or proteasome release.

We then performed three-dimensional deconvolution on Z-stack images from RPM-labeled HeLa cells (Fig. 3*A*) to minimize noise from out of focus sections. KRS and RPM staining exhibit a similar tangled-reticular pattern throughout the cell. A close look reveals punctuated areas where KRS and RPM extensively co-localize, as confirmed by statistical analysis (Pearson's coefficient higher than 0.5). By contrast, ribosomal P staining exhibits a distinct distribution, concentrating in cell periphery. This observation underscores our key finding that the MSC associates with ribosomes based on their translation activity.

To further explore this relationship, we used the proximity ligation assay (PLA), which is based on amplification of complementary DNA probes attached to different secondary antibodies used in immunofluorescence (29). Amplification requires that the two secondary Abs reside within 40 nm of each other. The anti-ribosomal P antibodies we used are specific for a cross-reactive, highly conserved epitope present on P0, P1, and P2 ribosome subunits. These proteins form a flexible stalk near the ribosome aminoacyl-tRNA binding (A) site (30). The anti-KRS/anti-ribosomal P combination gave obvious amplification with the expected ER staining pattern (Fig. 3*B*), mostly at the cell periphery. Combining RPM and PLA assays further demonstrated the interaction of KRS with translating ribosomes (in this case, the specificity of the PLA is clearly demonstrated by the complete absence of staining when cells are not exposed to Puro prior to processing, Fig. 3*C*). However, the reduced number of fluorescent dots suggests that only a fraction of the MSC is located within 40 nm of the ribosome stalk. Based on these observations, we conclude that first, the MSC and FRS are recruited to or near actively translating ribosomes in the DRC, and second, upon translation inhibition, the MSC partitions into a Dig soluble compartment.

MSC Is Recruited to Viral Translation Factories—If ARSs are selectively recruited to translating ribosomes, then they should localize to active translation sites in cells. To test this idea, we extended prior findings that in vaccinia virus (VV) infected cells; translation is almost exclusively limited to viral factories, *i.e.* sites of viral transcription, DNA synthesis and assembly (31). Four hours post-infection, viral factories are easily visualized as juxtanuclear DNA-containing bodies (Fig. 4*A*). Prior to Dig extraction, KRS is moderately concentrated in factories. Dig treatment reveals that KRS, MRS, and EPRS are largely concentrated in viral factories (Fig. 4*B*). Immunoblots of sucrose gradient fractions show that VV infection does not significantly modify MSC composition, expression, or association with polysomes (supplemental Fig. S3*A*), confirming that KRS, EPRS, and MRS staining reflect the intracellular distribution of the MSC.

Puro staining of VV-infected cells confirms that translation in the DRC occurs nearly exclusively in viral factories (Fig. 4*C*, *arrowheads*). MRS localization in factories (Fig. 4*D*) starkly contrasts with the heavy staining of idle ribosomes outside factories. Importantly, SRS is concentrated in VV factories, yet is still removed by Dig extraction (Fig. 4*E*). YRS, another "free" ARS, is resistant to Dig extraction and concentrates in VV factories (supplemental Fig. S3*B*).

To examine whether MSC recruitment to factories results from association with viral proteins, we performed 1D LC MS/MS mass spectrometry analysis on affinity purified MSC from enriched sucrose gradient fractions (supplemental Table S2). This failed to reveal peptides derived from viral proteins, consistent with the idea that the MSC is recruited to translating ribosomes, regardless of host *versus* viral origin of the mRNA. These findings fortify our conclusion that the MSC and at least some of the "free" ARSs are actively recruited to the vicinity of actively translating ribosomes.

Cellular Response to Chemical Stress Underscores the Close Relationship between the MSC and Translation Machinery—Cellular stress is known to greatly modify translation. Severe chemical stress results in the generation of stress granules that contain mRNA and translational components, acting as both a storage depot for future translation and a triaging station for preserving *versus* degrading mRNA. We induced stress granule formation by treating cells with sodium arsenite (As), as confirmed by staining cells for Hur, a stress-induced RNA binding protein that defines stress-granules (32) (Fig. 5*A*), As-treatment redistributed the MSC, as demonstrated using KRS as a proxy. KRS was re-localized around stress granules, co-localizing with the ribosomal large subunit. We confirmed this observation using MRS and eIF3η, another stress-granules marker (supplemental Fig. S4*A*). Parallel sucrose gradient analysis confirmed polysome dissociation and redistribution of FRS mainly into monosome fractions (Fig. 6*A*). Surprisingly, although translation arrest affected MSC sedimentation, its profile was clearly distinct from FRS. Rather that shift up in the density gradient, the MSC sedimented more rapidly, suggesting the MSC maintains association with some components of the translation machinery after stress-induced translation inhibition.

To probe the relationship between MSC and stress granules we infected HeLa cells with a recombinant Semliki Forest Virus (SFV) expressing IAV nucleoprotein (NP). SFV induces stress granules in conjunction with a nearly complete shutdown of host mRNA translation (33). SFV-NP infected cells demonstrate nearly complete translational shutdown by RPM

FIGURE 1. **MSC colocalizes with ribosomes.** *A*, HeLa cell extracts fractionated on sucrose gradients were immunoblotted to detect members of MSC (MRS and KRS), FRS, SRS or ribosomal proteins (P2 for the large ribosomal subunit, S3 for the small ribosomal subunit). Immunoblot signals were quantitated using Image J and graphed as percent of total recovered. *B* as in *A*, but the gradient is pooled into 3 regions, region 1 for soluble/uncomplexed proteins; region 2 for free MSC-containing fractions; region 3 for polysome fractions. Regions 2 and 3 were re-centrifuged to pellet protein complexes. *C*, immunofluorescence of anti-KRS (*green*) and Ribo P (*red*) Abs in fixed and permeabilized HeLa cells demonstrate extensive co-localization as quantitated by Van Steensel's Cross Correlation Coefficient (CCF) and Pearson's coefficient (shown) each greater than 0.75. Bar scale, 10 μm. *D* as in *C*, but HeLa cells were treated with Dig prior to fixation to remove soluble cytosolic proteins. Bar scale, 10 μm. *E* as in *C* and *D* but using antibodies specific for KRS (*green*) or SRS (*red*). Bar scale, 10 μm.

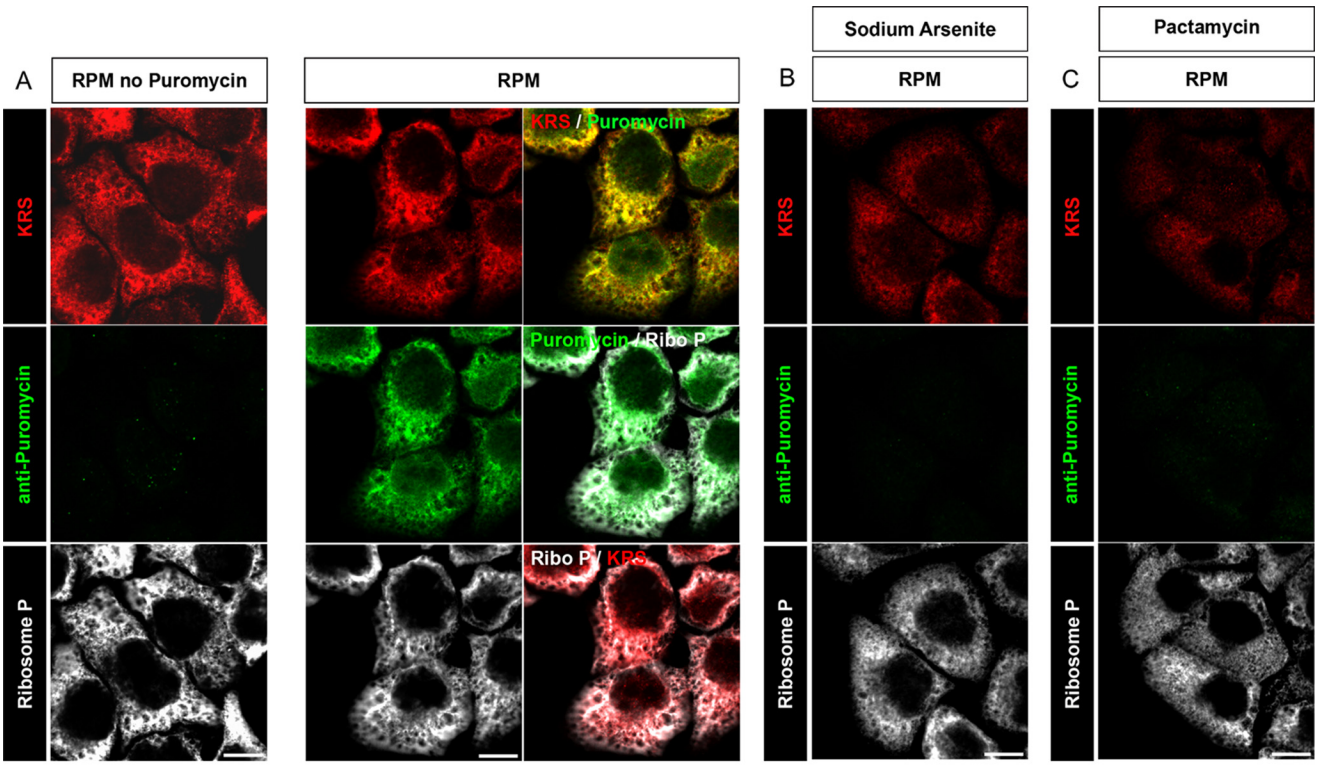
A
RPM no Puromycin
RPM
KRS
anti-Puromycin
Ribosome P
KRS / Puromycin
Puromycin / Ribo P
Ribo P / KRS
B
Sodium Arsenite
RPM
C
Pactamycin
RPM

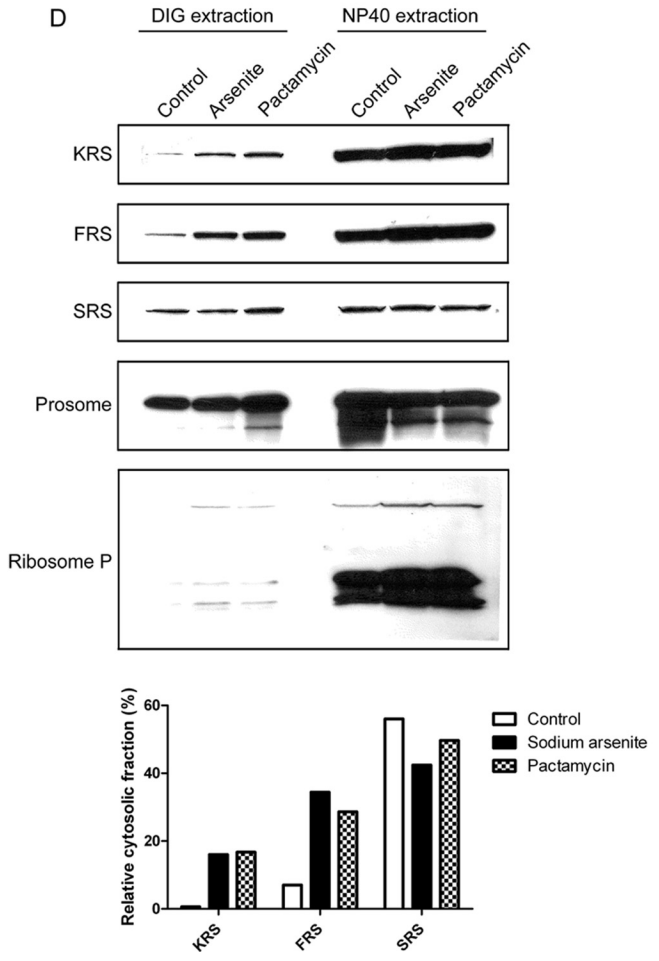
D
DIG extraction
NP40 extraction
Control
Arsenite
Pactamycin
Control
Arsenite
Pactamycin
KRS
FRS
SRS
Prosome
Ribosome P
Relative cytosolic fraction (%)
60
40
20
0
KRS
FRS
SRS
Control
Sodium arsenite
Pactamycin

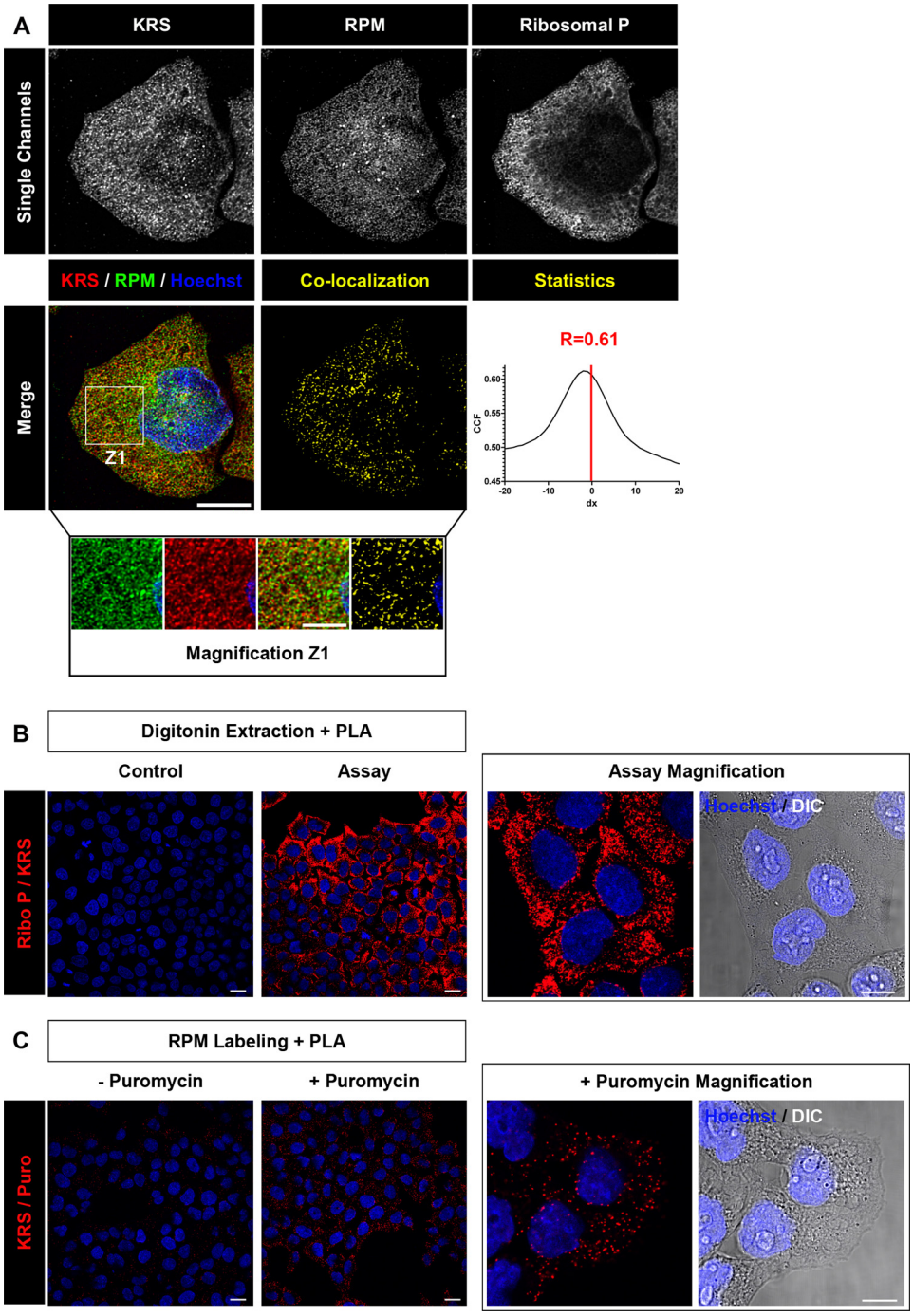

FIGURE 3. **MSC localizes with 40 nM of the ribosome A-site.** *A*, deconvolved images of HeLa cell labeled with RPM. KRS and RPM demonstrate extensive co-localization as quantitated by Van Steensel's CCF greater than 0.75 and Pearson's coefficient (*R*) greater than 0.5. Bar scale, 10 μm, 5 μm for Z1. *B*, ribo P/KRS PLA following Dig extraction. One primary antibody was omitted for the control sample. *C*, combined PLA RPM using Ribo P/Puro or KRS/Puro. Puromycin was omitted in the control sample.

(supplemental Fig. S4*B*) coincident with stress granule formation (supplemental Fig. S4*C*). The few remaining foci of translation co-localize with NP, consistent with the idea that SFV translation occurs at these sites (supplemental Fig. S4*B*). Importantly, with the exception of these foci, translation inhibition correlates with a nearly almost complete release of

FIGURE 2. **MSC concentrates in cellular translation sites.** *A*, HeLa cells were pulsed (or not) with puromycin and CHX to label translating ribosomes and extracted with Dig to remove free puromycin and cytosolic components. Cells were then fixed and permeabilized and stained for KRS, puromycin or ribosomal P proteins. In the absence of puromycin, no anti-puromycin staining was observed above background levels with secondary Ab alone, confirming the specificity of RPM. After a puromycin pulse, puromycin co-localizes with KRS and Ribo P. Bar scale, 10 μm. *B* and *C*, HeLa cells treated for 30 min with either with 500 μM sodium arsenite or with pactamycin no longer stain via RPM, demonstrating its specificity for translating ribosomes. Bar scale, 10 μm. *D*, HeLa exposed to arsenite or pactamycin were analyzed by immunoblotting for the indicated protein after Dig (cytosol only) or Nonidet P-40 extraction (*Cytosol + DRC*). Graph shows ImageJ quantitation of immunoblot signal, using the proteasome signal (*Prosome*) to normalize the amount of extract loaded in each lane.

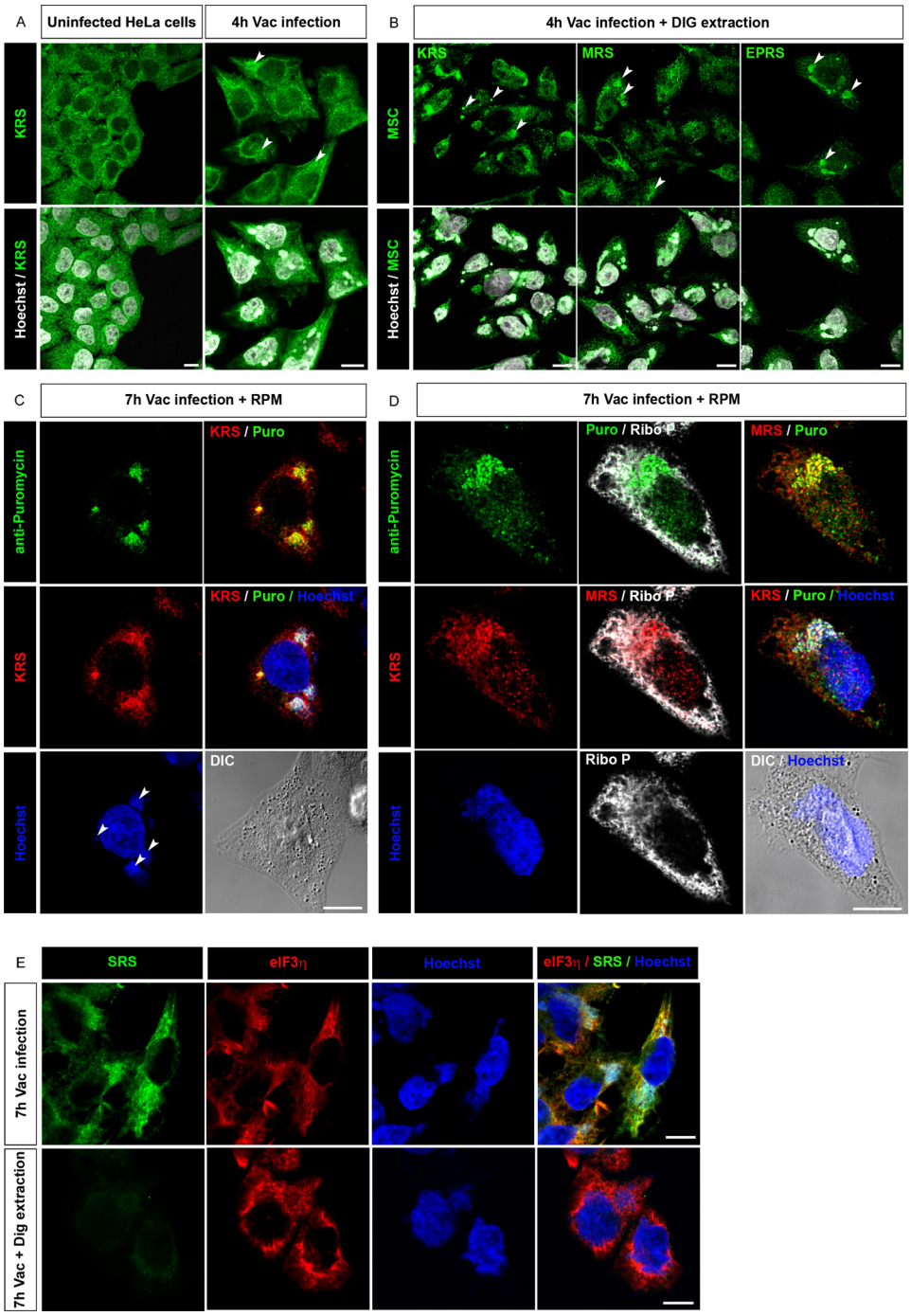

FIGURE 4. **MSC dynamically localizes to VV factories.** HeLa cells infected with VV for 4 h were fixed (*A*) or Dig extracted prior to fixation (*B*) and staining with the anti-ARS Abs indicated. Cytosolic Hoechst 3358 staining identifies viral DNA in factories (*arrowheads*). Bar scale, 10 μm. *C*, to obtain larger factories, cells were infected for 7 h with VV, and then pulsed with puromycin, extracted with Dig prior to fixation and stained for puromycin and the anti-ARS Ab indicated. Bar scale, 10 μm. *C* and *D*, *E*, after 7 h VV infection, cells were extracted or not with Dig prior to fixation and stained with Abs specific for SRS or eIF3η. Bar scale, 10 μm.

MSC and ribosomes from the ER-associated DRC (Fig. 5*B*). By staining for Hur and KRS, we confirmed that the MSC is concentrated in SFV-induced stress granules.

These findings suggest that stress granules may form in the center of active translation sites. To test this idea, we treated VV-infected cells with As after factories had formed. Indeed, Hur positive stress granules containing ribosomes and KRS formed co-incident with VV factories, and typically represented the largest stress granules in infected cells (Fig. 5*C*). Based on these data, we conclude first, that stress granule formation is related to local translation activity, and second, that the MSC behaves similar to other translational machinery in concentrating in stress granules.

MSC Binds to mRNA—What recruits the MSC to the vicinity of actively translating ribosomes? The difference in the sedimentation profiles of FRS and the MSC suggests that MSC associates with a rapidly sedimenting non-ribosomal substance. Strikingly, while As induced stress of HeLa cells results

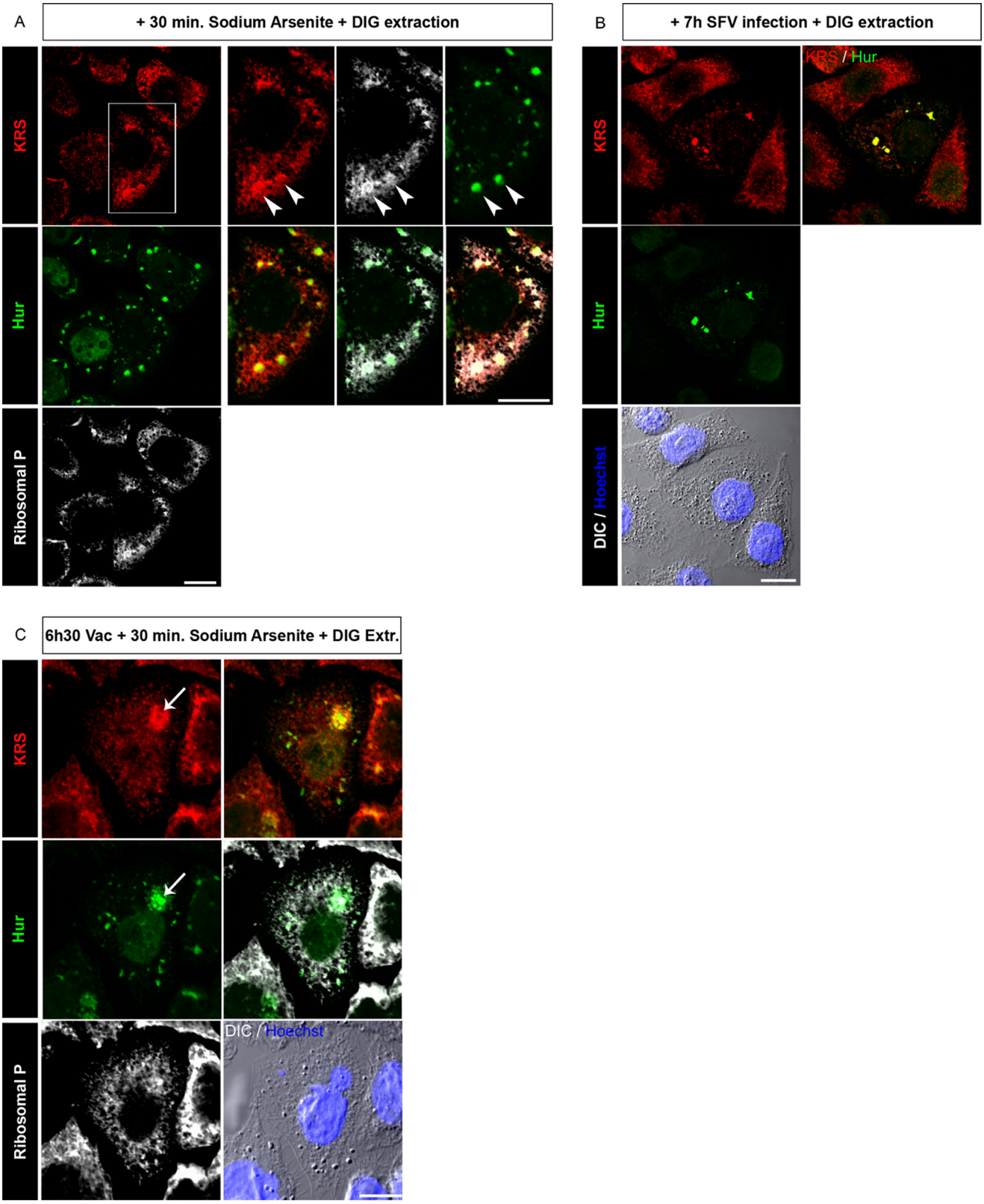

FIGURE 5. **MSC is recruited to stress granules.** *A*, HeLa cells were treated for 30 min with 500 μM of sodium arsenite before being extracted by Dig and stained for KRS, Hur, and Ribo P. High magnification zoom shows clearly stress granules with concentrated Ribo P and KRS (*arrowheads*). Bar scale, 10 μm. *B*, HeLa cells infected with Semliki Forest Virus for 7 h prior to Dig extraction and fixation. The SFV-infected cell in the center of the field contains cytosolic Hur-positive stress granules. Bar scale, 10 μm. *C*, HeLa cells infected with VV for 6.5 h, treated for 30 min with sodium arsenite, and extracted with Dig. *Arrow* indicates a mature factory containing large Hur-labeled stress granules. Bar scale, 10 μm.

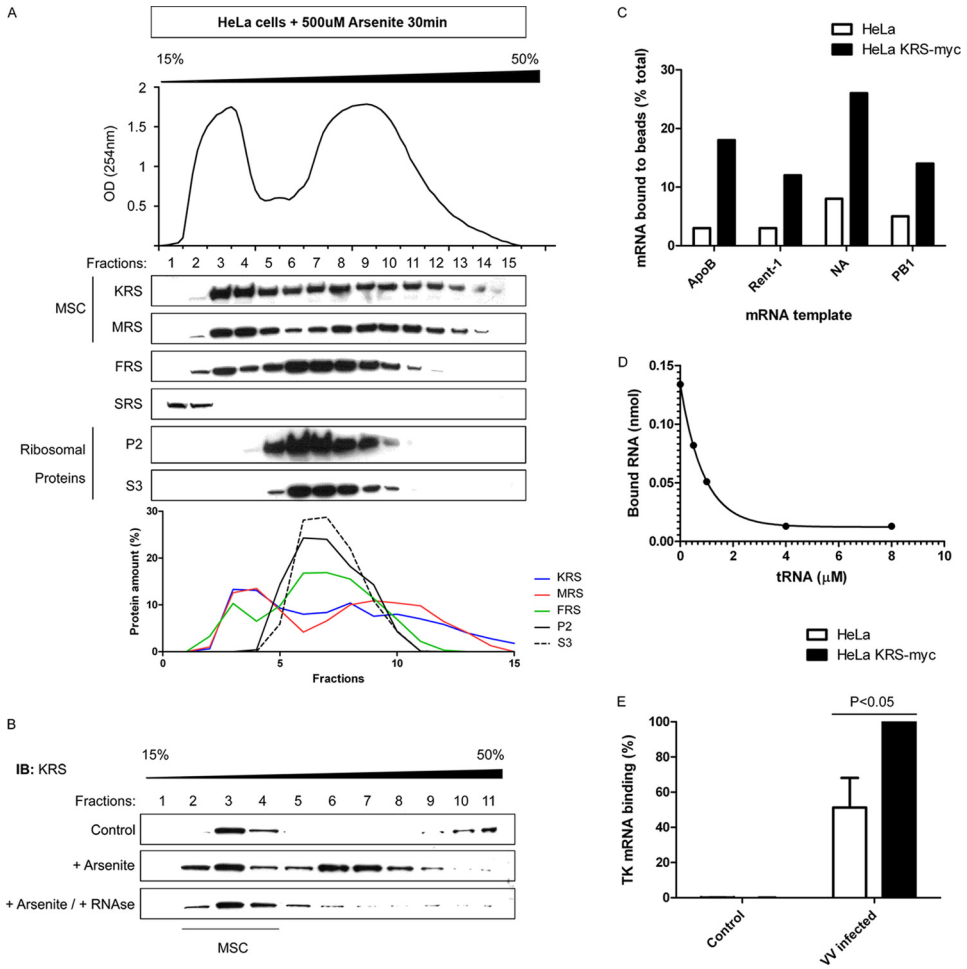

FIGURE 6. **MSC associates with mRNA.** *A*, HeLa cells were treated for 30 min with 500 μM of sodium arsenite before being analyzed as in Fig. 1*A* by sucrose gradient fractionation and immunoblotting. *B*, as in *panel A*, but lysates were treated with RNase prior to fractionation. *C*, four different protein-free ^{32}P-labeled RNA species synthesized by *in vitro* transcription were incubated with *control* anti-Myc tag Ab beads (incubated with MSC containing sucrose fractions from normal HeLa cells) or anti-Myc tag Ab beads containing immobilized MSC (sucrose fractions from myc-KRS expressing HeLa cells), and the amount of bound mRNA quantitated by scintillation counting. *D*, apoB [^{32}P]mRNA (at [13 nM]) binding to bead bound-MSC competing with tRNA for binding as indicated. Background binding on control beads was subtracted for each condition. 50% inhibition required 610 nM tRNA, demonstrating a 47-fold lower affinity of tRNA *versus* ApoB mRNA for MSC. *E*, HeLa cells or KRS-myc expressing HeLa cells were infected for 7 h with VV. Then the same purification procedure in *C* was performed. Total RNA from HeLa (control) and KRS-myc (containing MSC) beads was extracted, and quantitative RT-PCR was performed using primers for tVV-encoded thymidine kinase mRNA.

in a shift of FRS toward the monosome fraction in sucrose gradients, the MSC shifts to heavier fractions devoid of ribosomes, but still rich in RNA as shown by the OD at 260 nm (Fig. 6*A*), consistent with the possible association of the MSC with mRNA.

To test this idea, we treated extracts with RNase prior to fractionation. This shifted MSC sedimentation to the value expected for the free complex (Fig. 6*B*), demonstrating the RNA-dependent nature of MSC sedimentation. To more directly demonstrate MSC association with RNA, we added protein-free ^{32}P-labeled RNAs synthesized by *in vitro* transcription to anti-Myc tag Ab beads bound to MSC via Myc epitope-tagged-KRS (described below). Each of two viral and cellular mRNAs tested bound to MSC at high levels (Fig. 6*C*). The specificity of this interaction is demonstrated by the large increase over binding to identical beads loaded with cell extracts lacking Myc-tagged MSC. RNA binding cannot be trivially attributed to nonspecific association with any form of tRNA, because an 80-fold molar excess of unlabeled yeast tRNA is required to reduce radiolabeled mRNA by 50% (Fig. 6*D*).

To directly demonstrate *in cellulo* the binding of MSC to specific mRNAs, we infected HeLa cells or HeLa expressing KRS-myc with VV. We then purified Myc-tagged MSC using anti-Myc tag Ab beads, extracted bead-associated RNA, and performed a quantitative RT-PCR (Fig. 6*E*). VV thymidine kinase (TK) mRNA was present in Myc-MAC-tagged samples at twice the background values obtained using control HeLa cell samples.

These data demonstrate that in addition to binding tRNA, MSC binds mRNA through a non-competing site, providing a molecular basis for MSC delivery to translating ribosomes. Moreover, RNA binding would explain MSC behavior following chemical- and virus-induced stress. We propose that MSC is delivered to stress granules bound to host RNA, and localizes to viral factories due to viral degradation of host mRNA and binding to viral mRNA, which is highly concentrated in viral factories (31).

MSC-Ribosome Stoichiometry—Our findings demonstrate that the MSC is recruited to translating ribosomes, most likely by binding mRNA. To better understand the relationship between ribosomes and the MSC, we quantitated the MSC copy number per cell. To this end, we generated a HeLa cell line constitutively expressing Myc epitope-tagged KRS (Fig. S2A) (34), and confirmed by mass spectrometry analysis that anti-Myc Ab-purified MSC contains each of the 11 defined components (supplemental Fig. S2*B* and Table S2). We then used the purified complex as a standard for immunoblotting of total cell lysates with anti-KRS Ab (supplemental Fig. S2*C*). Because ~90% of KRS is present in the MSC (Fig. 1), KRS is a valid proxy for the MSC itself. Relating the blotting signal to the standard curve revealed an average copy number of 10^7 KRS per cell, equivalent to 9×10^6 assembled MSC per cell; three times the published number of ribosomes per HeLa cell (35). The ~3:1 stoichiometry of MSC and ribosomes, along with the binding of the MSC to mRNA is consistent with the idea that MSC function (and local tRNA supply) can be modulated on a ribosome-by-ribosome basis, and provides a foundation for deeper understanding the compartmentalized aspects of translation.

DISCUSSION

Using contemporary proteomic technology, we extend prior studies regarding the association of ribosomes with ARSs, and clearly demonstrate that FRS and each of the nine ARSs of the MSC co-sediment with polysomes in sucrose gradients, while the other 10 ARSs are not detected. Consistent with previous studies (36), immunoblots demonstrate that nearly all FRS associates with ribosomes. By contrast, only a minor fraction of the MSC co-sediments with ribosomes in sucrose gradients. This observation is consistent with our immunofluorescence findings indicating that a fraction of MSC extensively co-localizes with translating ribosomes although the rest of the MSC pool is concentrated nearby. The PLA data further support a close physical relationship between a fraction of the MSC and ribosomes in cells. This confirms and extends prior findings that the MSC and selected soluble ARSs are in the close vicinity of ribosomes, as determined by immunoelectron microscopy (37), and that the significant fraction of the MSC insoluble in 0.1% TX100 co-localizes with the ER by immunofluorescence (38).

Our most important finding is that MSC recruitment to translation sites is dynamic, a finding made possible by the application of RPM to studying ARS cell biology. The findings are particularly striking with VV-infection, where puromycylation and ARSs are nearly exclusively located in viral factories, despite the abundance of VV-silenced ribosomes elsewhere in the cytoplasm. Notably, co-localization of ARS with translating ribosomes extends to "free" ARSs such as SRS (co-localizing with KRS, Fig. 1*D*), and YRS (supplemental Fig. S3*B*). Although it seems likely that the eight other ARS are similarly recruited to translation sites, this remains to be established experimentally. MSC binding to mRNA provides a mechanism for translation-dependent association, a possibility supported by the reported mRNA binding properties of SRS and QRS (present in the MSC) (39, 40). Still, additional studies are needed to rule out the contribution of other potential mechanisms.

Mirande and co-workers (11) recently used fluorescence recovery after photobleaching (FRAP) to show that the mobility of the MSC (identified by expressing MRS-GFP) and also a free ARS (NRS-GFP) is highly limited in living cells. MRS mobility was increased by disrupting the actin cytoskeleton with latrunculin A. Although this finding was interpreted in the context of ribosome association with the actin cytoskeleton (41), ER organization is also impacted by latrunculin A (42), and the relatively modest effect of latrunculin A on MRS mobility might also reflect increased mobility of ER associated ribosomes. Further, given our finding that MSC associates with mRNA, the involvement of the cytoskeleton in mRNA transport in cells (43) potentially further complicates interpretation of the FRAP findings. It is of obvious interest to examine the effect of translational shutdown on ARS mobility in future FRAP studies.

We show that like many translation components, the MSC segregates in stress granules that form in cells experiencing chemical or viral stress. Because stress granules function as a mRNA depot, a parsimonious explanation is that MSC localization is based on its mRNA binding capacity.

There is increasing evidence that a significant fraction or mRNA are zip-coded to specific regions in cells for localized translation (44). Spirin (45) proposed that mRNAs acquire the factors required for their own translation, forming ribonucleoprotein particles he termed "informosomes." We propose that MSC binding to mRNA contributes to mRNA targeting and translation efficiency. Although we show that mRNA binding is much tighter than MSC binding to tRNA, high local tRNA concentrations in translation domains could release MSC from mRNA in the vicinity of translating ribosomes. Such localized translation potentially provides another level of translational control: the potential for mRNA-specific alterations in MSC specificity.

With the Pan laboratory, we recently reported that numerous stimuli leading to an oxidative stress response modifies ARS (probably the MSC itself) specificity to lead to a high rate of Met for other amino acids (up to 14% of Met bound to non-cognate tRNAs) (19). Based on the known role of Met in protecting proteins against oxidative damage (46), we proposed that misacylation-based Met substitution provides protection for nascent proteins synthesized in oxidatively stressed cells. This mechanism would have maximal impact if Met-substitution occurred in a non-random manner. Although a 14% misacylation rate seems high, it results in only a single Met substitution in an average sized protein (500 residues). A specific association of MSC with certain mRNAs could provide a potential means for modifying Met-misacylation on a gene product specific basis to provide the optimal Met substitutions for proteins that would maximally benefit.

Finally, the intimate relationship of ARSs with translating ribosomes extends the considerable existing evidence supporting the concept of channeled translation (8), and provides an explanation for the finding that that free RRS cannot substitute for MSC-associated RRS despite maintaining normal levels of total Arg-tRNA (7). The 3:1 stoichiometry of MSC and ribosomes suggests that within the translation compartment each ribosome is associated with one to two MSCs. The remarkably low copy number of tRNAs per ribosome (10–25) along with

10-fold (or more) differences in tRNA copy number implies that each compartment contains >20 ribosomes (48) to possess a complete set of tRNAs. This would represent 4 mRNAs per compartment, at an average polysome size of 5 ribosomes/mRNA.

Given the mounting evidence for mRNA zip coding (even now in bacteria (49)) and specialization of the components of the translation and folding machinery, it is of great interest to examine how specific and general translation events *e.g.* the generation of peptides for immunosurveillance (47, 50), are spatially and functionally segregated.

Acknowledgments—We thank Glennys Reynoso for providing outstanding technical support. We thank Sanford P. Markey (NIMH, Bethesda, MD) for invaluable discussions and Jeffrey A. Kowalak (NIMH, Bethesda, MD) who did a separate analysis on the data to confirm the mass spectrometry results.

REFERENCES

1. Schimmel, P. R., and Söll, D. (1979) *Annu. Rev. Biochem.* **48,** 601–648
2. Bandyopadhyay, A. K., and Deutscher, M. P. (1971) *J. Mol. Biol.* **60,** 113–122
3. Kellermann, O., Brevet, A., Tonetti, H., and Waller, J. P. (1979) *Eur. J. Biochem.* **99,** 541–550
4. Quevillon, S., Robinson, J. C., Berthonneau, E., Siatecka, M., and Mirande, M. (1999) *J. Mol. Biol.* **285,** 183–195
5. Kerjan, P., Cerini, C., Sémériva, M., and Mirande, M. (1994) *Biochim. Biophys. Acta.* **1199,** 293–297
6. Park, S. G., Ewalt, K. L., and Kim, S. (2005) *Trends. Biochem. Sci.* **30,** 569–574
7. Kyriacou, S. V., and Deutscher, M. P. (2008) *Mol. Cell.* **29,** 419–427
8. Stapulionis, R., and Deutscher, M. P. (1995) *Proc. Natl. Acad. Sci. U.S.A.* **92,** 7158–7161
9. Hampel, A., and Enger, M. D. (1973) *J. Mol. Biol.* **79,** 285–293
10. Ussery, M. A., Tanaka, W. K., and Hardesty, B. (1977) *Eur. J. Biochem.* **72,** 491–500
11. Kaminska, M., Havrylenko, S., Decottignies, P., Le Maréchal, P., Negrutskii, B., and Mirande, M. (2009) *J. Biol. Chem.* **284,** 13746–13754
12. Blobel, G. (2000) *Chembiochem.* **1,** 86–102
13. Stephens, S. B., and Nicchitta, C. V. (2008) *Mol. Biol. Cell.* **19,** 623–632
14. Pyhtila, B., Zheng, T., Lager, P. J., Keene, J. D., Reedy, M. C., and Nicchitta, C. V. (2008) *RNA.* **14,** 445–453
15. Lerner, R. S., and Nicchitta, C. V. (2006) *Rna.* **12,** 775–789
16. Stephens, S. B., Dodd, R. D., Brewer, J. W., Lager, P. J., Keene, J. D., and Nicchitta, C. V. (2005) *Mol. Biol. Cell.* **16,** 5819–5831
17. Potter, M. D., and Nicchitta, C. V. (2002) *J. Biol. Chem.* **277,** 23314–23320
18. Stephens, S. B., and Nicchitta, C. V. (2007) *Methods Enzymol.* **431,** 47–60
19. Netzer, N., Goodenbour, J. M., David, A., Dittmar, K. A., Jones, R. B., Schneider, J. R., Boone, D., Eves, E. M., Rosner, M. R., Gibbs, J. S., Embry, A., Dolan, B., Das, S., Hickman, H. D., Berglund, P., Bennink, J. R., Yewdell, J. W., and Pan, T. (2009) *Nature* **462,** 522–526
20. Schmidt, E. K., Clavarino, G., Ceppi, M., and Pierre, P. (2009) *Nat. Methods.* **6,** 275–277
21. Lelouard, H., Gatti, E., Cappello, F., Gresser, O., Camosseto, V., and Pierre, P. (2002) *Nature* **417,** 177–182
22. McFarland, M. A., Ellis, C. E., Markey, S. P., and Nussbaum, R. L. (2008) *Mol. Cell. Proteomics.* **7,** 2123–2137
23. Slotta, D. J., McFarland, M. A., and Markey, S. P. (2010) *Proteomics* **16,** 3035–3039
24. Robinson, J. C., Kerjan, P., and Mirande, M. (2000) *J. Mol. Biol.* **304,** 983–994
25. Mosyak, L., Reshetnikova, L., Goldgur, Y., Delarue, M., and Safro, M. G. (1995) *Nat. Struct. Biol.* **2,** 537–547
26. Geels, J., Bont, W. S., and Rezelman, G. (1971) *Arch. Biochem. Biophys.* **144,** 773–774
27. Kappen, L. S., Suzuki, H., and Goldberg, I. H. (1973) *Proc. Natl. Acad. Sci. U.S.A.* **70,** 22–26
28. Kedersha, N. L., Gupta, M., Li, W., Miller, I., and Anderson, P. (1999) *J. Cell Biol.* **147,** 1431–1442
29. Fredriksson, S., Gullberg, M., Jarvius, J., Olsson, C., Pietras, K., Gústafsdóttir, S. M., Ostman, A., and Landegren, U. (2002) *Nat. Biotechnol.* **20,** 473–477
30. Remacha, M., Jimenez-Diaz, A., Santos, C., Briones, E., Zambrano, R., Rodriguez Gabriel, M. A., Guarinos, E., and Ballesta, J. P. (1995) *Biochem. Cell Biol.* **73,** 959–968
31. Katsafanas, G. C., and Moss, B. (2007) *Cell Host. Microbe.* **2,** 221–228
32. Kedersha, N., and Anderson, P. (2002) *Biochem. Soc. Trans.* **30,** 963–969
33. McInerney, G. M., Kedersha, N. L., Kaufman, R. J., Anderson, P., and Liljeström, P. (2005) *Mol. Biol. Cell.* **16,** 3753–3763
34. Park, S. G., Kim, H. J., Min, Y. H., Choi, E. C., Shin, Y. K., Park, B. J., Lee, S. W., and Kim, S. (2005) *Proc. Natl. Acad. Sci. U.S.A.* **102,** 6356–6361
35. Duncan, R., and Hershey, J. W. (1983) *J. Biol. Chem.* **258,** 7228–7235
36. Pailliez, J. P., and Waller, J. P. (1984) *J. Biol. Chem.* **259,** 15491–15496
37. Popenko, V. I., Ivanova, J. L., Cherny, N. E., Filonenko, V. V., Beresten, S. F., Wolfson, A. D., and Kisselev, L. L. (1994) *Eur. J. Cell Biol.* **65,** 60–69
38. Mirande, M., Le Corre, D., Louvard, D., Reggio, H., Pailliez, J. P., and Waller, J. P. (1985) *Exp. Cell Res.* **156,** 91–102
39. Miseta, A., Woodley, C. L., Greenberg, J. R., and Slobin, L. I. (1991) *J. Biol. Chem.* **266,** 19158–19161
40. Schray, B., and Knippers, R. (1991) *Nucleic Acids Res.* **19,** 5307–5312
41. Hovland, R., Hesketh, J. E., and Pryme, I. F. (1996) *Int. J. Biochem. Cell Biol.* **28,** 1089–1105
42. Griffing, L. R. (2010) *Biochem. Soc. Trans.* **38,** 747–753
43. Jansen, R. P. (1999) *FASEB. J.* **13,** 455–466
44. Holt, C. E., and Bullock, S. L. (2009) *Science* **326,** 1212–1216
45. Spirin, A. S. (1978) *FEBS Letts.* **88,** 15–17
46. Luo, S., and Levine, R. L. (2009) *FASEB J.* **23,** 464–472
47. Lev, A., Princiotta, M. F., Zanker, D., Takeda, K., Gibbs, J. S., Kumagai, C., Waffarn, E., Dolan, B. P., Burgevin, A., Van Endert, P., Chen, W., Bennink, J. R., and Yewdell, J. W. *Proc. Natl. Acad. Sci. U.S.A.* **107,** 6964–6969
48. Princiotta, M. F., Finzi, D., Qian, S. B., Gibbs, J., Schuchmann, S., Buttgereit, F., Bennink, J. R., and Yewdell, J. W. (2003) *Immunity* **18,** 343–354
49. Nevo-Dinur, K., Nussbaum-Shochat, A., Ben-Yehuda, S., and Amster-Choder, O. (2011) *Science* **331,** 1081–1084
50. Yewdell, J. W., and Nicchitta, C. V. (2006) *Trends Immunol.* **27,** 368–373